ISBN: 978-3-95450-241-7 ISSN: 2673-5350 doi:10.18429/JACoW-IBIC2022-TUP43

REQUIREMENTS AND STATUS OF PETRA IV FAST ORBIT FEEDBACK SYSTEM

S.H. Mirza*, A. Aloev, H.T. Duhme, B. Dursun, A. Eichler, S. Jablonski,
J. Klute, F. Ludwig, S. Pfeiffer, H. Schlarb, B. Szczepanski
Deutsches Elektronen-Synchrotron DESY, Hamburg, Germany
G. Rehm, Helmholtz-Zentrum Berlin für Materialien und Energie/BESSYII, Berlin, Germany

Abstract

PETRA IV is the upcoming low-emittance, 6 GeV, fourth-generation light source at DESY Hamburg. It is based upon a six-bend achromat lattice with additional beamlines as compared to PETRA III. Stringent stability of the electron beam orbit in the ring will be required to achieve a diffraction-limited photon beam quality. In this regard, the requirements and the proposed topology of the global orbit feedback system are discussed for expected perturbations. An initial analysis based upon system requirements, design and modelling of the subsystems of the orbit feedback system is also presented.

INTRODUCTION

Multi-bend achromat (MBA) lattice design in fourth-generation light sources provides the possibility of achieving a high degree of transverse coherence and brightness of photon beams by generating extremely low emittance electron beams. But the effort must be complemented by the transverse orbit stability against dipolar perturbations arising within the ring and from ground motion. Moreover, the transverse orbit stability requirement has drastically increased in the fourth-generation light sources also due to the smaller size of the electron beam in both transverse planes.

The upcoming PETRA IV of DESY Hamburg, which is an upgrade of the existing ring of PETRA III will have a six-bend achromat lattice [1] with additional beamlines having transverse beam position and pointing angle stability requirement of 5% to 10% of the electron beam size and divergence, respectively. A fast orbit feedback (FOFB) system is being developed to achieve disturbance rejection up to 1 kHz on the closed orbit. The main strategy for designing the FOFB system is to identify the requirements and design the subsystems around these requirements using lattice-based simulations.

The required performance criteria for the fast orbit correction is defined by the beam size and divergence at insertion devices (given in Table 1).

Even a generally accepted target of keeping RMS variation of electron beam position and pointing angle to 10% of RMS beam size and divergence [2] requires stabilization of 297 nm and 100 nrad (RMS) in the vertical plane of PETRA IV. The beam size and divergence are given with $\sigma = \sqrt{\beta\epsilon + \sigma_E^2\eta^2}$ and $\sigma' = \sqrt{\frac{\epsilon}{\beta}}$, where ϵ and β are the emittance and beam size, respectively. The energy spread

* sajjad.hussain.mirza@desy.de

Table 1: Electron Beam Parameters at IDs

Parameter	Value
$\beta_{x,y}$ (m), standard cell	2.2
$\beta_{x,y}$ (m), flagship IDs	4
Nat. emittance $\epsilon_{x,y}$ (pm rad)	20, 4
Beam size $\sigma_{x,y}$ (µm), standard cell	6.6, 2.97
Beam div. $\sigma'_{x,y}$ (µrad), standard cell	3.02, 1.34
Beam size $\sigma_{x,y}$ (µm), flagship IDs	8.9, 3.98
Beam div. $\sigma'_{x,y}$ (µrad), flagship IDs	2.23, 1.0

σ_E and the dispersion η is assumed to be zero at the location of IDs. The reuse of the old tunnel of PETRA III will come with relatively larger static and dynamic errors [3]; a stability task force was formed to model the error spectrum. The ground motion is expected to be below 100 Hz, but a disturbance rejection bandwidth of 1 kHz is targeted to achieve reasonable attenuation on the lower side of the frequency spectrum where most of the disturbances are expected. This is necessary to achieve the above-mentioned stability criteria, which further requires a latency-optimized system. The update rate of the closed loop is planned to be 130 kHz (equal to the revolution frequency) to reduce the latency in the closed loop. In this case, the betatron frequencies ($\nu_x = 23.43$ kHz and $\nu_y = 35.156$ kHz) cannot be disregarded in the FOFB modelling, because they are within the Nyquist sampling frequency and they may be in the region where the sensitivity function (transfer function from disturbance to output) could have a magnitude larger than 1.

This contribution discusses the proposed topology for the global FOFB system. In addition, analytical modeling of the subsystems is presented, which plays an important role in their design and in identifying the technical challenges to achieve 1 kHz disturbance rejection for SISO simulation.

PROPOSED TOPOLOGY FOR THE FOFB SYSTEM

FOFB system for PETRA IV is planned to perform orbit correction for the full range of disturbance spectrum, i.e. from quasi-DC to high frequency (1 kHz). The slow correctors distributed along the ring will correct large and slow orbit offset drifts. The FOFB system will correct fast perturbations referenced to the orbit maintained by slow correctors during machine commissioning. A total of 789 beam position monitors (BPMs) and 322 fast correctors in the vertical plane, and 200 fast correctors in the horizontal plane will

ISBN: 978-3-95450-241-7 ISSN: 2673-5350 doi:10.18429/JACoW-IBIC2022-TUP43

be available for the FOFB. The FOFB system for PETRA IV is planned to have an extended star topology which will have 1 global central node marked as "GLO" between supply building 12 and 13 and 15 local nodes (LOC), see Fig. 1.

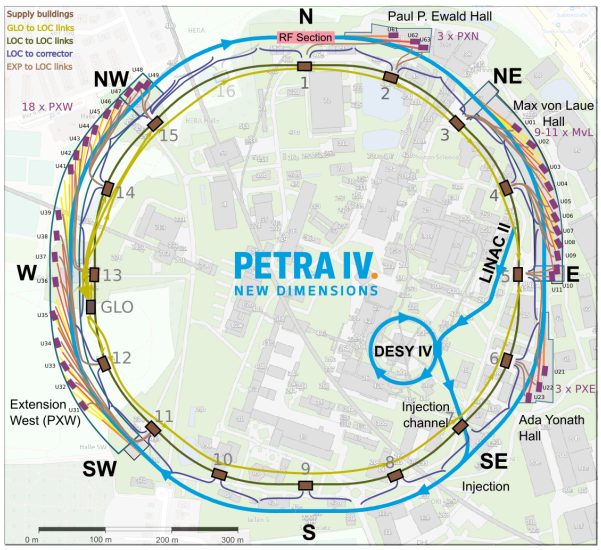

Figure 1: Supply buildings across the ring to serve as local stations for BPM and corrector data collection and distribution.

BPM crates and power supply (PS) racks will be peripheral nodes for each local star. BPM crates are planned in the MicroTCA.4 form factor, housing multiple BPM processors coupled with a data aggregation AMC for transferring the corresponding BPM data to LOC. PS units are planned to be distributed into racks with a single optical link per rack. Various options such as optical splitters are being considered to distribute the data locally to the individual PSs. The GLO and LOC are planned as similar hardware, which will also have the MicroTCA.4 form factor. GLO will have bidirectional optical links up to 1.2 km long with all 15 LOCs. Each LOC will be connected to the local BPM crates and local PS racks with optical links. Optical links to both neighbouring LOCs (upstream and downstream) and experimental stations are also considered. Figure 2 shows the simplified block diagram for central data processing.

The main idea behind such a topology is establishing a latency-optimized global system. Data propagation within the MicroTCA.4 backplanes is latency-optimized in order of 270 ns, while the optical cable paths are bandwidth-optimized. Data transfer times are up to 6 µs for the longest communication path between LOC and GLO, and we expect a latency of less than one microsecond for each local communication, i.e. LOC to PS and BPM.

ANALYTICAL MODELLING OF SUBSYSTEMS

This section describes the main transfer characteristics of individual subsystems in the signal chain for the FOFB system. The starting point will be the signal detection by

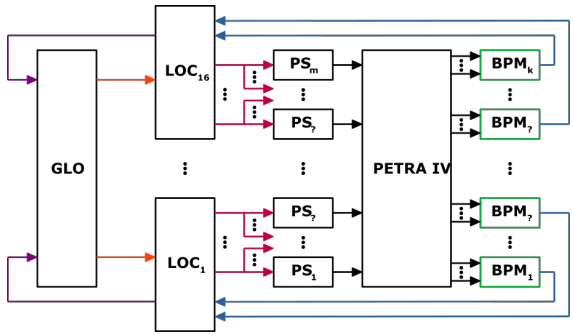

Figure 2: Simplified block diagram for central data processing around the PETRAIV ring. Optical communication links, displayed as colored lines, from up to k=789 BPMs via up to 16 LOCs and 1 GLO to about 522 PS, locally distributed over the corresponding LOC.

the BPM, followed by the corrector power supply up to the considered beam dynamics.

Beam Position Monitor

Button BPMs with four distributed pickups will be located around the ring. The BPM electronics is based on Libera Brilliance+ system [4] providing turn-by-turn data with a resolution of at least 100 nm and an update rate of 130 kHz [5]. This data should be free of switching artifacts and with a maximum latency of 3 turns, i.e. latency of about 23 µs. The latency, orbit resolution, and noise modelling of the BPM electronics are the most important elements for the simulation.

Corrector Power Supply

The power supply design is not finalized yet, but the considered option includes two paths: slow regulation (feedback based) up to a maximum of a few hundred Hertz for mainly slow drift compensation and fast uncontrolled (feed-forward) regulation for fast correction to overcome mismatch in the current readback using DCCT at the PS output. This solution provides low latency, the update rate of 130 kHz, no feedback, but a lead-lag component is required for the fast corrector coil to reach at least 1.3 kHz open-loop bandwidth.

Cable and Corrector Magnets

Cables with lengths up to 200 m are required between the corrector power supplies and the magnets to keep the power electronics outside the tunnel. This puts special demands on the cable itself, like low losses, radiation hardness and other aspects discussed in the following.

All 3 horizontal and 2 out of 4 vertical fast correctors per cell (in the current lattice of PETRA IV) overlap the locations of slow correctors. So the combined AC/DC corrector magnet design is proposed capable of 800 µrad DC deflection (twice the value predicted by static error analysis [3]) and 30 µrad integrated deflection up to 1 kHz. The aperture diameter of 25 mm and length no longer than 150 mm are the design parameters from the lattice point-of-view. The proposed design is based on the layout of the 8-pole correc-

ISBN: 978-3-95450-241-7 ISSN: 2673-5350 doi:10.18429/JACoW-IBIC2022-TUP43

tor magnet for APS-U [6]. This layout allows improved field quality for both deflection planes created by the main and auxiliary coils. The schematic is shown in Fig. 3.

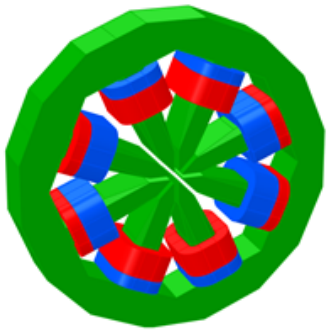

Figure 3: Combined corrector layout for PETRA IV. The main and auxiliary coils are represented by inner and outer coils, respectively, with blue representing horizontal correctors and red representing vertical correctors.

At a certain ratio of ampere-turns in these coils, it is possible to minimize the 3rd and 5th harmonics (b_3 and b_5). In practice, main and auxiliary coils are connected in series. The number of turns is chosen as a compromise between the field quality, inductance and maximum current. For example, Table 2 shows relative (to dipole) integrated harmonics, maximum current and inductance for 65/27 and 70/29 turns in the main and auxiliary coils.

Table 2: Number of turns in main and auxiliary coils, maximum DC current I (A) and inductance L of fast corrector magnets. The integrated harmonics are given relative to the main dipole harmonic b_1 (values in 10^{-4}).

Turns	L [mH]	I [A]	$\mathbf{b_3}$	$\mathbf{b_5}$	$\mathbf{b_7}$	$\mathbf{b_0}$
65/27	23.0	22.3	2.5	0.90	278	−26.6
70/29	26.4	20.7	−3.2	−1.0	278	−26.6

The bandwidth of magnet core (eddy current effect) is modelled to be 10 kHz based upon measurements of similar correctors at APS-U (private communication). First simulations of PS, cable and magnet depict an additional challenge in terms of cable-magnet resonance, dominated by large magnet inductance and capacitance of such a long cable. In first order, this is given as a series LC circuit as

$$f_{\text{res}} = \frac{1}{2\pi\sqrt{L_{\text{mag}} C_{\text{cable}} l_{\text{cable}}}}\,, \tag{1}$$

where L_{mag} is the magnet coil inductance, C_{cable} is the cable capacitance per meter and l_{cable} is the length of the cable. Figure 4 shows the corresponding notch in the source current at 8.3 kHz. This notch creates uncertainty between source current and magnet current at frequencies around the notch. Hence a closed-loop current controller shall be limited to a few hundred Hz. Therefore, the proposed solution is to use a feed-forward circuit for kHz regime based upon a closed-loop of global FOFB beam-based system while a closed-loop

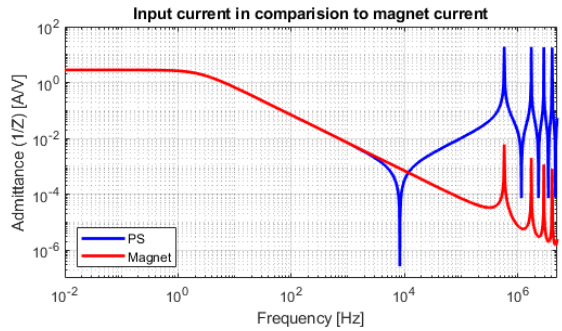

Figure 4: The notch in current in the coaxial cable connected with magnet coil, at 8.3 kHz seen by the source point of view.

current controller up to 100 Hz only for drift compensation of the set point. In this case, the overall open-loop bandwidth shall significantly reduce and currently, estimation (based upon current design considerations) is 1.3 kHz. The corrector coil transfer function (voltage to current) shall be overtaken by the action of this PS with a lead-lag component. Furthermore, the cable resonances are found to be $f_{\text{peak}} = \frac{cN_{1,3,5,\ldots}}{4\sqrt{\epsilon_r \mu_r} l}$, where c is the speed of light, ϵ_r is the relative permittivity, and μ_r is the relative permeability. The peaks are shifted towards lower frequency by the increase of cable length and should not overlap with the multiples of betatron tunes.

Vacuum Chamber

The eddy currents in the vacuum chamber placed inside an electromagnet act like a low-pass filter attenuating the magnetic field inside the chamber. If the skin depth of material is larger than the thickness of the chamber, its response can be modelled as a first order filter given as,

$$G_{vac} = \frac{\omega_0}{s+\omega_0},\ \omega_0 = \frac{1}{\tau},\ \tau = \frac{1}{2}\mu_0 \sigma a d \tag{2}$$

where, $\mu_0 = 4\pi\times10^{-7}$ H/m, σ is conductivity, a is the internal radius and d is the thickness of chamber [7]. In order to make the eddy current effects non-dominant, 1 mm thick stainless steel chamber of radius 10.5 mm is requested for the fast correctors (BW=17.8 kHz), contrary to the alternate option of copper (BW=770 Hz, for 0.5 mm thickness). Remark: inner coating might be necessary that can reduce the bandwidth down to 7 kHz. This aspect is currently under discussion for impedance matching and ignored for simulations presented here.

Beam Dynamics

Orbit Response Matrix The pseudo-inverse of the orbit response matrix (ORM) serves as the machine model for the calculation of the corrector settings for a given perturbed orbit. The elements of the ORM are given as,

$$R_{mn} = \frac{\sqrt{\beta_m \beta_n}}{2\sin(\pi Q)} \cos\left(Q\pi - |\mu_m - \mu_n|\right) \tag{3}$$

where β and μ denote the beta function and phase advance at BPM and corrector locations marked as m and n respectively,

ISBN: 978-3-95450-241-7 ISSN: 2673-5350 doi:10.18429/JACoW-IBIC2022-TUP43

in the given plane. Q is the coherent betatron tune of the storage ring. The condition numbers of PETRA IV ORMs (ratio of highest to lowest singular values) are 322.8 and 765 for horizontal and vertical planes, respectively.

Betatron Oscillations

The betatron excitation needs to be taken into account as mentioned in the introduction section. The transfer function model between a corrector and a BPM for betatron excitation is given as,

$$H_{mn} = \sqrt{\beta_m \beta_n}\ \mathrm{Im}\left(\frac{e^{j(\mu_m - \mu_n)}}{s + \frac{1}{\tau} - j\nu}\right) \tag{4}$$

where τ is the damping time constant and $\nu_{x,y} = 2\pi Q_{x,y} f_{\mathrm{rev}}$, [8]. For SISO simulation, it is modelled as a damped second-order low-pass filter with $H = \frac{p_1 p_2}{(s-p_1)(s-p_2)}$, where $p_i = -(\frac{1}{\tau} \pm j\omega_t)$.

Synchrotron Oscillations

The beam's momentum deviation ΔP with respect to nominal momentum P_0 produces a closed orbit distortion through the dispersion function D as $x_D = \frac{\Delta P}{P_0} D$. The momentum deviation is not a constant but rather oscillates with the synchrotron oscillation frequency resulting into "fast" orbit oscillations [9] making the synchrotron frequency relevant for PETRA IV FOFB system where the $\Omega_t = 600$ Hz (within the disturbance rejection bandwidth).

Single-Input-Single-Output Simulations

A first-hand estimation of the full open-loop transfer function and delay budget for the FOFB system is made based upon analytical modelling of the subsystems discussed above and depicted in Fig. 5. The estimation is done for the worst-case scenario (for maximum delay paths from LOC to GLO stations). Figure 6 shows the simulated Bode plots for the vacuum chamber, corrector magnet eddy current effect, power supply and their combined transfer function with a net open-loop bandwidth of 1.26 kHz. Similarly, a total delay of 83 µs is estimated ($\tau_{\mathrm{d,BPMs}}$=23 µs, $\tau_{\mathrm{d,controller}}$=30 µs, $\tau_{\mathrm{d,LOC\text{-}GLO}}$=15 µs, $\tau_{\mathrm{d,PS\text{-}cable}}$=15 µs). Figure 6 also shows the total response adding the betatron resonance ($\nu_x = 23.43$ kHz and $\nu_y = 35.156$ kHz) with decay constants ($\tau_x = 17$ ms and $\tau_y = 22$ ms) for both planes, in

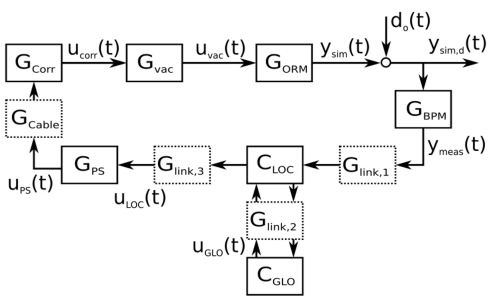

Figure 5: Closed-loop schematic of the FOFB system identifying the individual subsystems.

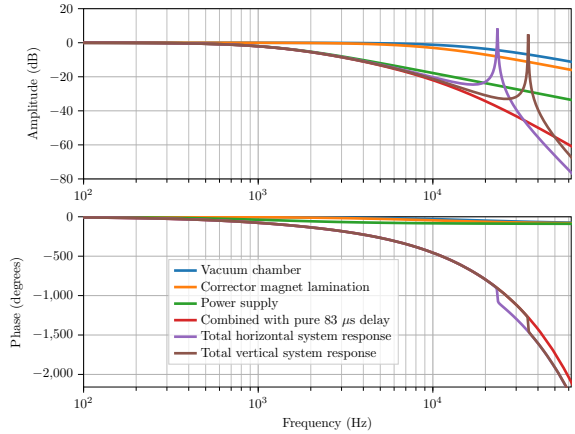

Figure 6: Open-loop transfer function of subsystems.

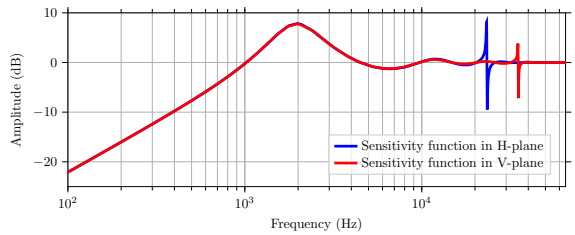

Figure 7: Disturbance-to-output sensitivity function

the absence of multi bunch feedback. The synchrotron oscillations are ignored in these simulations. The closed-loop simulation in the SISO domain is performed using a PI controller, with closed-loop bandwidth three times of open-loop bandwidth. Disturbance rejection of 1 kHz seems feasible as depicted by the disturbance-to-output sensitivity function in Fig. 7, for the subsystems described above.

SUMMARY

This paper presents a preliminary analysis of requirements and proposed topology for the global FOFB system for PETRA IV. Analytical subsystem modelling is also presented in order to evaluate the feasibility 1 kHz disturbance rejection bandwidth.

REFERENCES

[1] I. V. Agapov *et al.*, "PETRA IV Storage Ring Design", in *Proc. IPAC'22*, Bangkok, Thailand, Jun. 2022, pp. 1431–1434. doi:10.18429/JACoW-IPAC2022-TUPOMS014

[2] G. Rehm, "Achieving and measuring sub-micrometer beam stability at 3rd generation light sources", *J. Phys. Conf. Ser.*,vol. 425, p. 042001, 2013. doi:10.1088/1742-6596/425/4/042001

[3] T. Hellert *et al.*, "Error Analysis and Commissioning Simulation for the PETRA-IV Storage Ring", in *Proc. IPAC'22*, Bangkok, Thailand, Jun. 2022, pp. 1442–1444. doi:10.18429/JACoW-IPAC2022-TUPOMS018

[4] P. Paglovec *et al.*, "The RF BPM Electronics Concept and Developments for the PETRA IV project at DESY", MicroTCA Workshop (DESY), 2021. {https://bib-pubdb1.desy.de/record/473042}

ISBN: 978-3-95450-241-7 ISSN: 2673-5350 doi:10.18429/JACoW-IBIC2022-TUP43

[5] G. Kube *et al.*, "Upgrade of the BPM long term drift stabilization scheme based on external crossbar switching at PETRA III", presented at IBIC'22, Kraków, Poland, Sep. 2022, paper WEP08, this conference.

[6] M. Jaski, "APS Upgrade: Magnets", ASD Seminar, Apr. 2017. https://www.aps.anl.gov/files/APS-Uploads/ASDSeminars/2017/2017-04-12-Jaski.pdf

[7] B. Podobedov *et al.*, "Eddy Current Shielding by Electrically Thick Vacuum Chambers", in *Proc. PAC'09*, Vancouver, Canada, May 2009, paper TH5PFP083, pp. 3398–3400. https://jacow.org/PAC2009/papers/TH5PFP083.pdf

[8] Y. Cheng, "Dynamic Closed Orbit Correction", in *Proc. PAC'93*, Washington D.C., USA, Mar. 1993, pp. 2269–2271. https://jacow.org/p93/PDF/PAC1993_2269.PDF

[9] P. Kallakuri *et al.*, "Coupled bunch mode zero correction using orbit measurements and rf system phase feedback", *Phys. Rev. Accel. Beams*, vol. 25, p. 082801, 2022. doi:10.1103/PhysRevAccelBeams.25.082801